High Molecular Weight Polypropylene Nanospheres: Synthesis and Characterization

Pradip Paik,[1] Kamal K. Kar[1,2]

[1]*Advanced Nano Engineering Materials Laboratory, Materials Science Programme, Indian Institute of Technology, Kanpur 208016, India*
[2]*Advanced Nano Engineering Materials Laboratory, Department of Mechanical Engineering, Indian Institute of Technology, Kanpur 208016, India*

Received 1 August 2006; accepted 16 December 2006
DOI 10.1002/app.26177
Published online 10 April 2007 in Wiley InterScience (www.interscience.wiley.com).

ABSTRACT: The high molecular weight (MW) polypropylene with average particle size of 60 nm was synthesized by controlled growth mechanism using Ziegler–Natta catalyst. The atomic force microscopy (AFM), scanning electron microscopy (SEM), and transmission electron microscopy (TEM) studies showed that PP nanoparticles were spherical in shape. Structure and crystallinity were concomitantly studied through Fourier transform infrared spectroscopy and X-ray diffraction, respectively. It shows nanospherical PP particles with more crystallinity ($\sim$ 75%) compared with macrosized PP ($\sim$ 59%). In addition, differential scanning calorimetry studies revealed the finite particle size effect on T_g and the scale dependence T_g followed a first order exponential trend. As particle size goes down to nano- scale from macrosize, continuous elevation of T_g's were observed from -25 to -11°C. This phenomenon was directed to configuration entropy of single spherical nanoparticles of PP. The mechanical properties and surface roughness were also evaluated through AFM. At last, the properties of nanosized PP were compared with micron and macrosized particles. © 2007 Wiley Periodicals, Inc. J Appl Polym Sci 105: 1133–1143, 2007

Key words: polypropylene; nanosphere; high molecular weight; mechanical properties; morphology

INTRODUCTION

Dramatic advances to create nanoscale materials with the hope of eliminating our dependence on limiting, top-down technologies, that is high resolution lithography are observed in the last decade.[1] Again with the development of atomic force microscopy (AFM), controlled positioning of submicron particles is possible for inorganic materials like nanowires.[1] The formation and application of nanoparticles enjoy great popularity in academia and industries. Various approaches like sol-gel process, microemulsion technique, etc are used for the generation of inorganic nanoparticles. Now the question arises for organic polymeric materials, which are of very high molecular weight (MW) (weight–average molecular weight is more than 1×10^5).

Polypropylene (PP) is of particular interest because it has been extensively studied in macroscale and is one of the most essential polymers among the commodity thermoplastic materials. Special interest in PP nanospherical particles stems for their potential application in the areas of composite,[2–4] biotechnology,[5,6] powder technology,[7] optoelectronics,[8] catalytic support for bioreactor and for waste water treatment,[9,10] electrostatic enhancement application,[11,12] surface and coating technology,[13] etc. For instance, polymer particles with functionalized surfaces could add in the fabrication of nanoscale devices, smart sensing,[14] electrical,[15] and fluorescent[16] properties. In addition to that, it has been observed that PS (polystyrene) latex particles in their nano- and submicron size ranges (MW $<$ 20,000) have widely been used for nanostructure materials fabrication.[17–19] Polymer particles at submicron scales exhibit interesting properties i.e., photonic,[20,21] mechanical, optical, and electrooptical[22] in the various fields of industrial and biomedical applications because of the faster response to environmental change, which is again responsible for its minimum size, high surface to volume ratio, low surface tension, etc. Such exciting properties can advance the field of nanotechnology (MEMS/NEMS), a simultaneous development of new materials and design (e.g., nanopatterning). In spite of its tremendous importance of nanomaterials, not a single work has been carried out for PP. Another limitation of polymer particles at nanoscale is its extremely high MW and Van der Waals force of interaction. Till date it was not pos-

Correspondence to: K. K. Kar (kamalkk@iitk.ac.in).
Contract grant sponsor: Ministry of Human Resource Development, New Delhi, India.

Journal of Applied Polymer Science, Vol. 105, 1133–1143 (2007)

sible to prepare polymer particles at nanoscale without loosing its ultrahigh MW. Few polymers like polystyrene, polyethylene glycol, etc are available at nanoscale, but their MW is less than 20,000. The ability to manipulate single PP particles will lead researches to consider it as a promising candidate for nanostructure building blocks. In the last two decades, several techniques have evolved to prepare polymer particles to synthesize nanoscale materials and structure,[23–25] of which (1) micro- or miniemulsion polymerization,[26] (2) block copolymerization,[25,27–29] and (3) crosslinking polymerization[30] are among the most suited processes. Generally PP at macroscale is produced by Ziegler–Natta catalyst, metallocene catalysts, etc. In this context the objective of this research article is to synthesis high MW PP at nano- and microscale without sacrificing its high MW using Ziegler–Natta catalyst. The second objective is to characterize the polymer through particle size distribution and morphology using AFM, scanning electron microscopy (SEM), and transmission electron microscopy (TEM). It is well known that physical and mechanical properties of a polymer are dictated by morphology, which in turn, is influenced by the crystallization behavior of polymer. Crystallization behavior is strongly influenced by the average MW, MW distribution, stereoregularity, and processing behavior of polymers. Keeping this in mind, the next objective is to see the effect of nanosize on structure and crystallinity using X-ray diffraction (XRD). The dependence of glass transition temperature on the size has been investigated using differential scanning calorimetry (DSC). Investigation of surface roughness and micromechanical properties through AFM is another objective. Beside this, the results were also compared with macroscale.

MATERIALS AND METHODS

Synthesis of nano-, micron- and macrosized PP

High MW PP having particle sizes in micro and nanometer scale were prepared by Grignard reagent i.e., methyl magnesium chloride; propylene and hydrogen gases; trimethyl aluminum and titanium chloride; methanol and hydrochloric acid; and *n*-hexane, diethyl ether, xylene, dimethyl siloxane over a range of temperature from 30 to 160°C, pressure of 3–15 MPa, and shear rate of 0.2–200 rad/s. At first the catalyst was prepared from titanium chloride and trimethyl aluminum in *n*-hexane solvent. Then the catalyst, propylene, and hydrogen (here hydrogen acts as a chain terminating agent) are charged into the reactor at a pressure of 3–15 MPa, time of 12 h, and temperature of 70–90°C. The resulting mixture containing PP, *n*-hexane, propylene, and catalyst is heated at a temperature of 170°C to remove propylene monomer. The residue is then treated with methanol acidified with traces of hydrochloric acid to decompose and dissolve the catalyst. After that the polymer was centrifuged and washed with water. The solid mass was again dissolved in common solvents over a wide range of temperature from 0 to 160°C and shear rate of 0.2–200 rad/s to make a clear solution. The clear solution is cooled slowly with continuous stirring to form nano- and micron-sized polymers. The detailed methods are reported elsewhere.[31,32]

Infrared spectroscopy

The IR spectra of commercially available PP (i.e., macrosize) and PP particles were recorded using a BRUKER VECTOR22 Fourier transform infrared spectroscopy (FTIR) spectrometer at room temperature. For all samples, the scanned wave number range was 4000–500 cm^{-1}.

Atomic force microscopy

AFM was performed with a nanoscope equipment (Molecular Imaging) operating in AAC (Acoustic AC Mode). The instrument was equipped with an E-Scanner and commercial silicon tips cantilever (NSC 12 (c) from Mikro Masch, force constant of 0.6 N/m, resonance frequency of 150 KHz, and a tip diameter smaller than 20 nm) with a scan speed of 1.5–2.2 lines/s. Powder samples were dispersed in propen-2-ol and deposited on the mica substrate. Then the number average diameter (D_n) was calculated using eq. (1).[33]

$$D_n = \sum_i N_i D_i \Big/ \sum_i N_i \quad (1)$$

The distribution of particle size was calculated from 200 numbers of particles. The image background was mica.

Transmission electron microscopy

Particle size of the PP particles was also determined with a JEOL JEM-100CX transmission microscope. PP particles were dispersed in 25 mL of propen-2-ol. A drop of 2% phosphotungstic acid was added in the mixture. After proper dispersion through ultrasonication, a drop of this mixture was placed on a carbon coated copper grid of 400 mesh size. The particle diameters were measured directly from each transmission electron micrograph. Then the number average diameters (D_n) were calculated using Eq. (1). The distribution of particle size was calculated from 1000 numbers of particles.

X-ray diffraction

The powder XRD measurements were carried out at room temperature with a RICH SEIFERT ISO-DEBYEFLE 202 Diffractometer using CuKα (λ = 1.540598 E) radiation source at 30 kV and 20 mA, and scan rate was 3°/min between 2θ = 7° and 30°.

Scanning electron microscopy

The particle size and morphology of nanopolymer were also determined by using a FEI QUANTA 200 Scanning Electron Microscope (SEM). Prior to SEM studies, the samples were sputter coated with Au–Pd without touching the surface.

Differential scanning calorimetry

Thermal analyses of macro-, micro- and nanoparticles were done with Perkinelmer Diamon DSC instrument to calculate the glass transition temperature (T_g). The scanning rate was 10°C/min from 30 to 200°C. N_2 gas was used as an inert atmosphere to avoid degradation of PP. Before, DSC run, instrument was calibrated from 30 to 250°C using indium (T_m^0 = 156.6°C and ΔH_f^0 = 28.5 J/g) and zinc (T_m^o = 419.47°C and ΔH_f^o = 23.01 J/g). All the samples were encapsulated inside the Al pan and lid with mass of ~ 5 ± 0.1 mg for each experiment.

RESULTS AND DISCUSSION

Infrared spectra of crystalline polymers are complex due to the regular structure of the macromolecules. To simplify it, all spectra are classified into the four groups related to the various molecular structures: conformational band, stereoregularity band, regularity band, and crystallinity band.[34,35] Some absorption bands are very sensitive to the physical state of the samples. According to different origins, these sensitive bands are classified into two categories. One of these is related to the intramolecular forces in the crystal lattice, where the polymer molecules pack together on a regular three dimensional arrangement. This type of band is known as crystallinity band. The other type of band is related with the intramolecular vibration coupling within a single chain and known as regularity band or helix band. The conformational band and regularity band are easily observed for crystallized PP in the mid-infrared region. Figure 1 shows the FTIR spectra of PP nanoparticles. All of the 1370, 1301, 1254, 1219, 1161, 1103, 994, 975, 899, 840, and 810 cm^{-1} bands belong to the regularity bands.[34,35] They are associated with the different helical length of repeat unit (n). The minimum n values for appearance of bands at 975, 994, 840, and 1219 cm^{-1} are 5, 10, 12, and 14 monomer units in helical sequence, respectively. The higher the common unit, the more is the order degree of the corresponding regularity band. Concerning the 975 cm^{-1} band, it is not only attributed to the PP head to tail sequence of repeating units, but also associated with the presence of short helices. On the other hand, the band at 1453 cm^{-1} is assigned to asymmetric deformation vibration of the methyl group.[34,35] The FTIR spectrum of PP macroparticles is also included in the same Figure 1. It is very interesting to note that there is no difference in chemical structure between the nano- and macroparticles of PP.

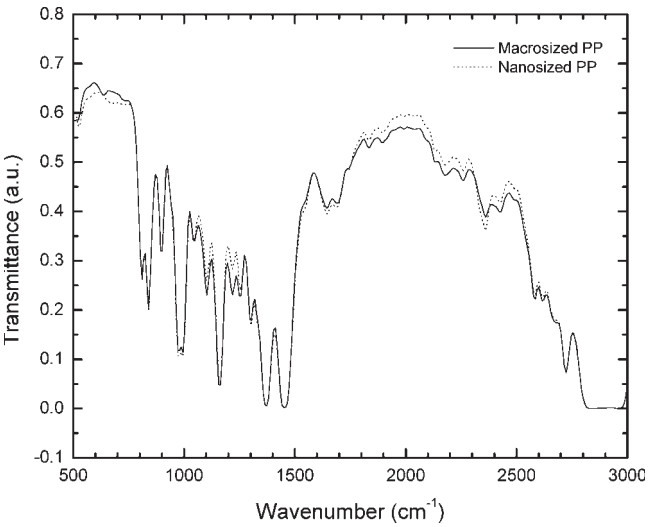

Figure 1 IR spectra of macro and nanosized PP.

Moreover, the PP nanoparticles are spherical in shape, which are confirmed from AFM, TEM, and SEM (Figs. 2–4). A supplementary craze to be noted, there is always a distribution of PP nanoparticles and these distributions are shown in the histogram [Figs. 2(c) and 3(c)]. AFM shows that maximum numbers of particles are of 40–60 nm, with a population of 65, and 100% in between 32 and 90 nm. From TEM, the maximum a number of particles are 44–55 nm sized with 61% population, and 100% in between 28 and 100 nm. Additional studies from SEM images (Fig. 4) show that the PP particles are spherical in morphology and particle sizes vary from 60 to 200 nm with an average particle size of 100 nm. These microscopy results show that there is no pronounced variation with the average particle size of spherical PP nanoparticles. It is also noticed from the microscopy analysis that nanoparticles are alienated from each other with uniquely patterned features.

The X-ray powder diffraction patterns of the PP micro- and nanoparticles having different particle size distribution were taken at room temperature

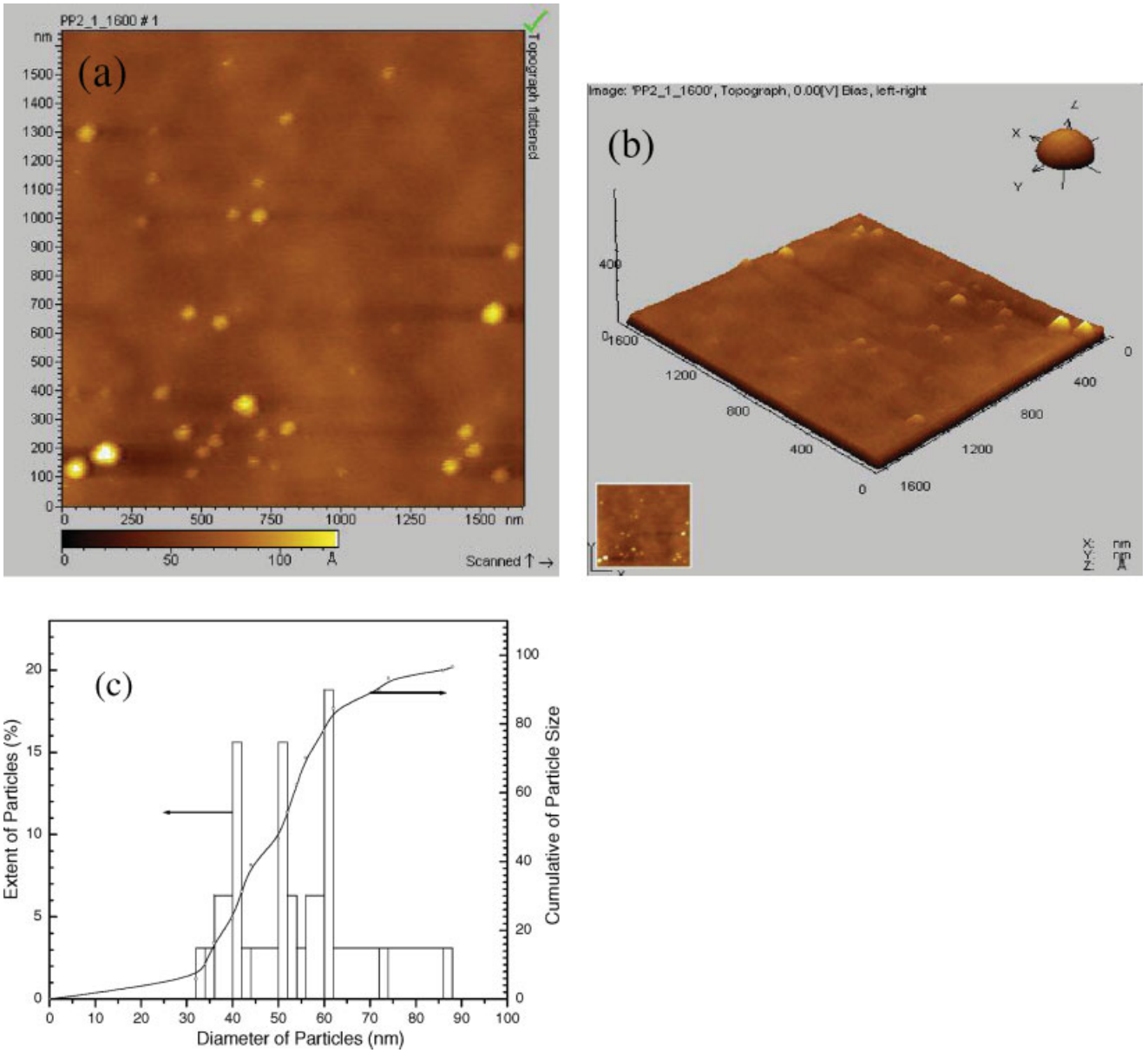

Figure 2 (a) Display of a 2D view of few of PP nanoparticles obtained from AFM topography. (b) Display of a 3D view of few of PP nanoparticles obtained from AFM topography. (c) Particle size distribution of nanosphere PP. [Color figure can be viewed in the online issue, which is available at www.interscience.wiley.com.]

(Fig. 5). The powder diffraction pattern for PP (average particle size ~ 20 μm) particles showed the strong diffraction peaks at 2θ ~ 14.3°, 17.1°, 18.7°, 21.3°, and 22.1°; for PP (average particle size ~10 μm) at 2θ ~ 14.3°, 17.2°, 18.8°, 21.4°, and 22.2°; for PP (average particle size ~ 5 μm) at 2θ ~ 14.4°, 17.2°, 18.7°, 21.4°, and 22.1°; for PP (average particle size ~ 1 μm) at 2θ ~ 14.3°, 17.2°, 18.7°, 21.4°, and 22.1°; and for PP (less than 500 nm) the same at 2θ ~ 14.3°, 17.2°, 18.7°, 21.3°, and 22.1°. The XRD at 2θ ~ 14.3°–14.4° is because of the 110(α) [Fig. 5(b)], at 2θ ~ 17.1–17.2° is because of the 040(α) [Fig. 5(c)], at 2θ ~ 18.7°–18.8° is because of the 130(α) [Fig. 5(c)], at 2θ ~ 21.3°–21.4° is because of the [111(α) + 301(β)] [Fig. 5(d)] and at 2θ ~ 22.1°–22.2° is because of the [131(α) + 041(α)] [Fig. 5(d)] reflection planes. From Figure 5(a), it is clear that the standard peak positions of PP micro- and nanoparticles remain unaltered with decrease in the particle size from micron to nanometer scale. It is also apparent from the XRD plots that the γ crystalline phase for which the X-ray reflection peaks appear at 2θ ~ 20.1° [117(γ) reflection plane] and 16.7° [008(γ) reflection plane] are completely absent here. It is important to point out that the γ crystalline phase generally appeared because of the average length of the crystallizable sequences, and the presence of γ crystalline phase is a indirect indication of degree of segregation of defects

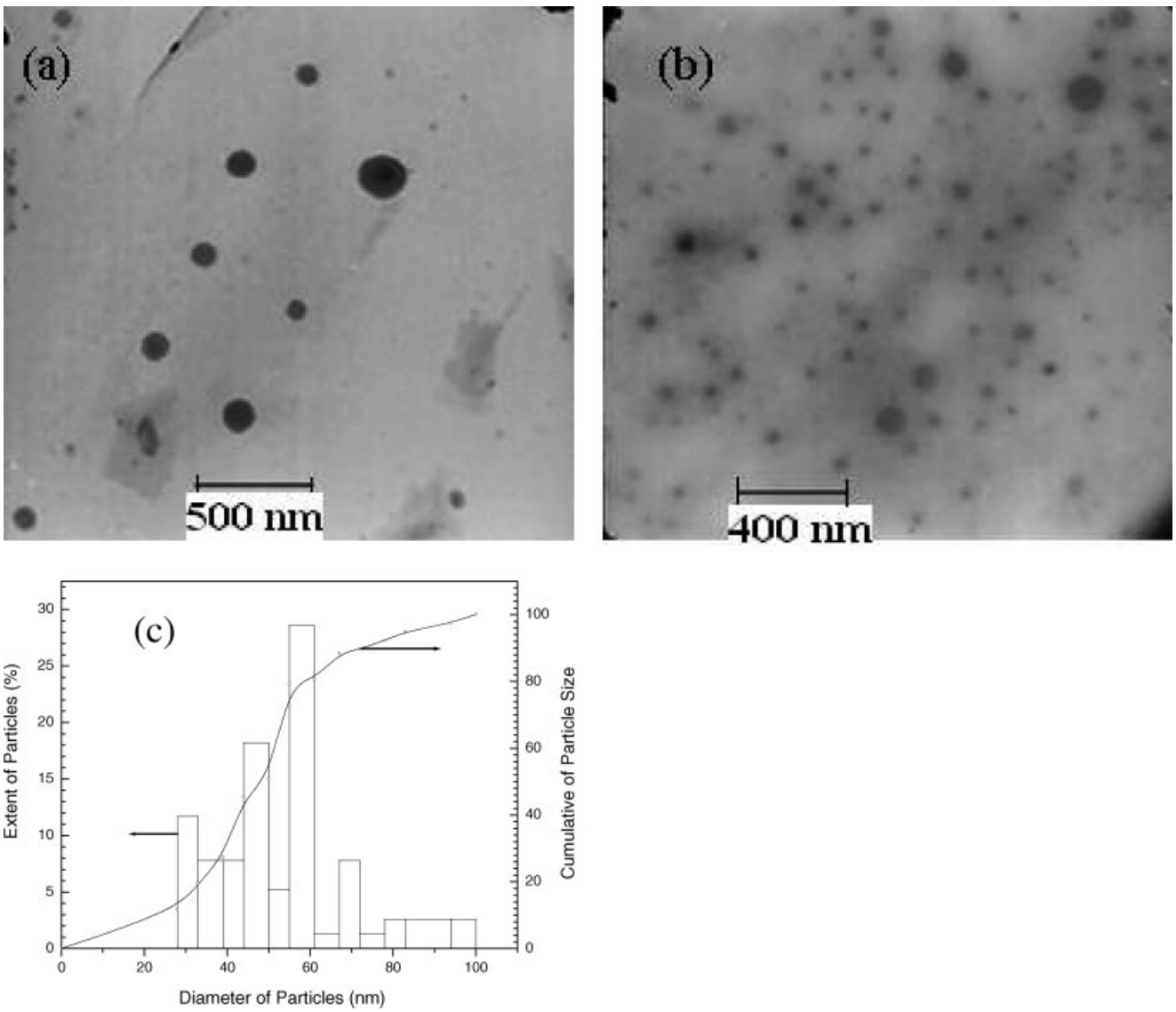

Figure 3 (a) TEM micrograph of PP particles. (b) Another TEM micrograph of PP particles. (c) Particle size distribution (histogram) of PP particles obtained from 3(a) and 3(b).

of the PP particles, where long and regular isotactic sequences are the cause of α crystalline phase formation.[36,37] Since, there are no γ crystalline phase peaks, it is confirmed that PP micro- and nanoparticles synthesized here are free of defects caused by γ phase.

The important characteristic peaks for the β-trigonal phase of PP particles are found at diffraction angles around $2\theta \sim 16^\circ$ and 21° corresponding to the reflection planes of (300) and (301), respectively. The peak at $2\theta \sim 16^\circ$ disappeared as particle size decreased to nanosize. The $2\theta \sim 21.3^\circ$ or $2\theta \sim 21.4^\circ$ peak for all PP particles, for instance, is a combination of both 110(α) and 301(β) planes [Fig. 5(c)]. The 301(β) plane reflection decreases as the 110(α) plane reflection increased as well as the β crystalline percentage decreased. The above results indicate the presence of little amount of β crystalline phase in PP micro- and nanoparticles.

The important characteristic peaks which appeared at $2\theta \sim 14.3^\circ$–14.4° is basically because of the 110(α) reflection plane [Fig. 5(b)], at $2\theta \sim 17.1^\circ$–17.2° is because of the 040(α) reflection plane, at $2\theta \sim 18.7^\circ$–18.8° is because of the 130(α) reflection plane [Fig. 5(c)], at $2\theta \sim 21.3^\circ$–21.4° is because of the [110(α) + 301(β)], and at $2\theta \sim 22.1^\circ$–22.2° is because of the [131(α) + 041(α)] reflection planes [Fig. 5(d)]. All the above peaks indicate the presence of extended amount of α-monoclinic crystalline phase. In comparison with the PP (20 μm), an obvious difference can be seen in PP (lass than 500 nm). The peak intensity for the crystalline phases even gradually increases from particle size PP (∼ 20 μm) to PP (lass than 500 nm). As the particle size gradually

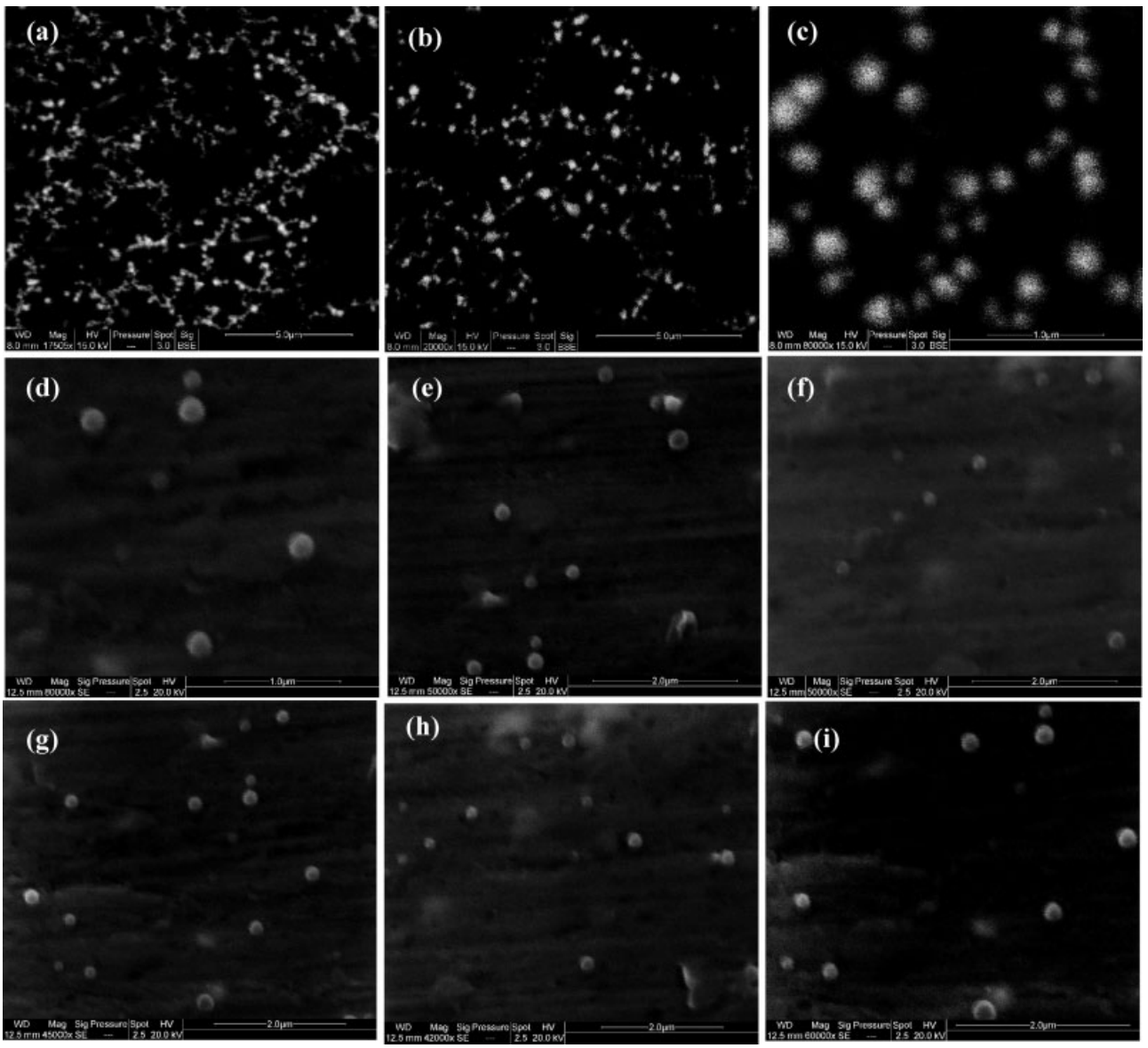

Figure 4 SEM photographs of PP particle. (Panels a–i stand for various magnification).

decreases, the extra orientation of crystalline planes (molecular chains) changed in favors of α-monoclinic phase.

A calculation for PP micro- and nanoparticles is given in Table I to show the relative enhancement of crystallinity with decrease in particle size for α and β crystalline phases. The crystallinity of the PP particles was calculated by Hermans and Weidingeer's equation[38] [eq. (2)].

$$\chi_c = \frac{A_c}{A_a + A_c} \tag{2}$$

where, A_c and A_a are the total crystalline and amorphous area obtained from XRD diffractogram, respectively. It shows that the relative increase in crystallinity for PP (less than 500 nm) of 110(α), 040(α), 130(α), 111(α) + 301(β), and 131(α) + 041(α), reflection planes are 23.0, 27.0, 26.5, 15.4, and 32.0%, respectively, with respect to the PP (∼ 20 μm) microparticles and the enhancement of crystallinity increases as the particle size decreased from micron to nanometer scale. These data clearly indicate that the α-monoclinic phase is being favored when the particle size of PP is in the nanometer range.

Figure 6 shows the XRD patterns of PP (∼ 20 μm), PP (∼ 10 μm), PP (∼ 5 μm), PP (∼ 1 μm), and PP (<500 nm) micro- and nanoparticles at the extended diffraction region from $2\theta \sim 23.5^\circ$–30°. It is noted that few new crystalline peaks appeared at $2\theta \sim 24.5^\circ$, 25.8°, and 28.8°. From Figure 6 it is

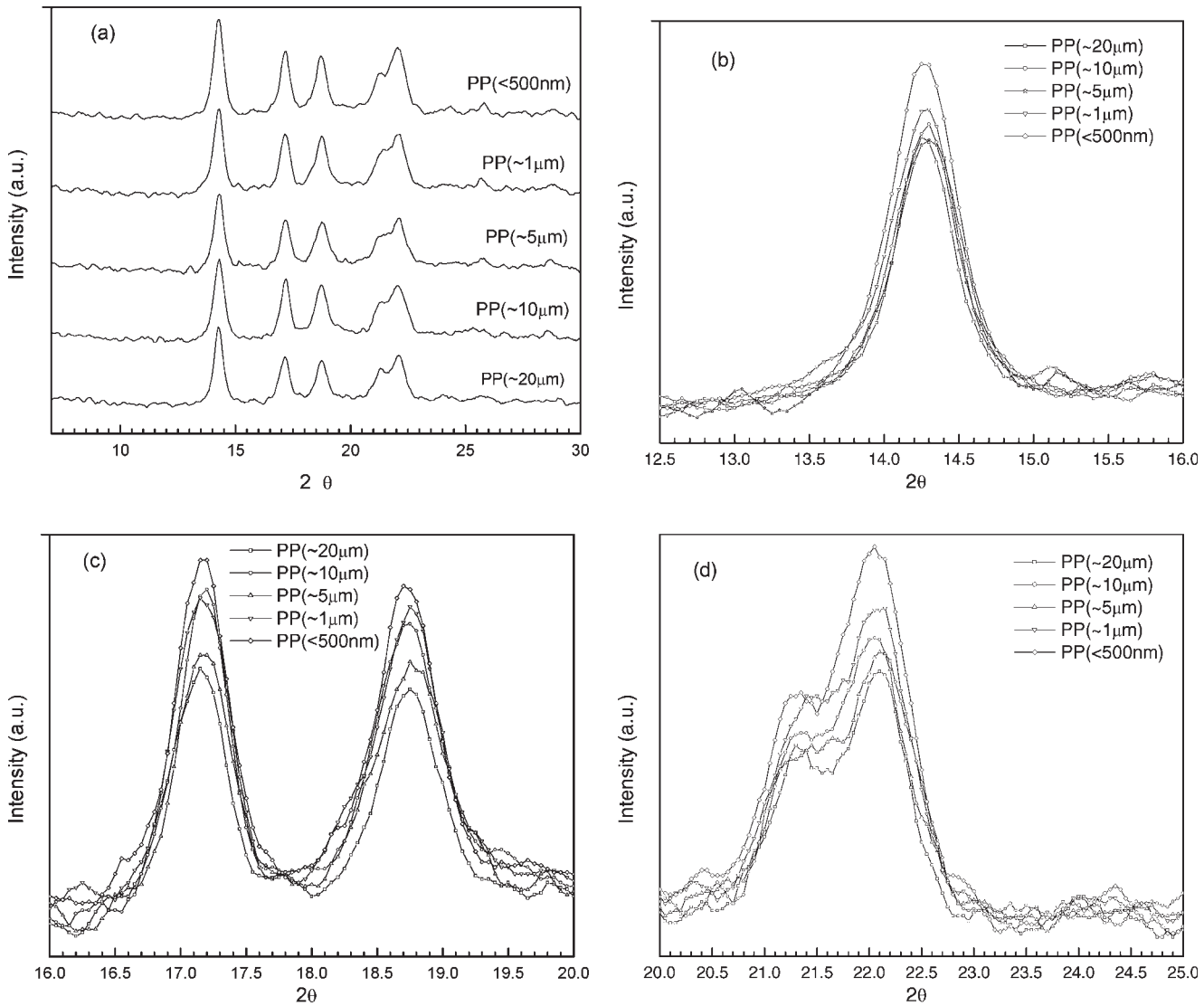

Figure 5 (a) X-ray powder diffraction patterns of PP particle in the range of $2\theta = 7^\circ$–30° (110(α)), (b) X-ray powder diffraction patterns of PP particles in the range of $2\theta = 12.5^\circ$–16° (040(α)), (c) X-ray powder diffraction patterns of PP particles in the range of ($2\theta = 16^\circ$–20° (130(α)), (d) X-ray powder diffraction patterns of PP particle in the range of $2\theta = 20^\circ$–25° (111(α) + 301(β) and 131 (α)+ 041(α)).

also noticed that the peaks intensity gradually increased from PP (∼ 20 μm) to PP (< 500 nm). The reasons for these results are due to the enhancement of α-monoclinic crystalline phase of PP particles. As the particle size gradually decreased, the extra orientation of crystalline plane (molecular chains) changed in favor of α-monoclinic phase towards right or left handed helical direction successively. This phenomenon occurred because of the azimuthal orientation of the molecular chains on successive planes. From extensive study, it is concluded that the diffractions at $2\theta \sim 24.5^\circ$, 25.8°, and 28.8° are because of the 131(α), 150(α) + 060(α), and 220(α) + 061(α), respectively. The new peak appearance and the enhancement of peak intensity are because of the higher crystallinity of PP nanoparticles relative to the microparticles. Table II shows the overall percentage of crystallinity of PP micro- and nanoparticles calculated from the eq. (2). When the particle size is reduced from PP (∼ 20 μm) to PP (less than 500 nm), the crystallinity is increased from 59 to 74%.

Figure 7 shows the experimentally determined glass transition temperature (T_g) of macro PP and PP having different particle sizes. It is significant to note that the T_g of PP spherical micro- and nanoparticles have higher values than that of macro PP particles. As the particle size decreases, T_g increases. For the macro PP particles the T_g is $\sim -25.3^\circ$C, and when the particle size is reduced to the less than 500 nm, T_g increases to -11°C. This dramatic change in the T_g for PP particles is quite

TABLE I
Crystallinity for PP Micro and Nanospherical Particles at Different Reflection Planes

α and β crystalline phase of PP particles	Crystallinity increased (%)		
	PP (~ 5 μm)	PP (~ 1 μm)	PP (less than 500 nm)
110(α)	1.5	21.0	23.0
040(α)	6.4	19.6	27.0
130(α)	6.2	19.8	26.5
$\bar{1}11$(α) + 301(β)	1.2	15.0	15.4
$\bar{1}31$(α) + 041(α)	4.0	15.0	32.0

These data were obtained from WRD profile shown in the Figure 5 and using Hermans and Weidingeer's equation. The calculation was done using reference peaks of PP (~ 20 μm).

TABLE II
Crystallinity of PP Micro- and Nanospherical Particles, Calculated from XRD Plots and Using Hermans and Weidingeer's Equation

PP particles	Crystallinity (%)
PP (~ 20 μm)	59
PP (~ 10 μm)	65
PP (~ 5 μm)	63
PP (~ 1 μm)	69
PP (< 500 nm)	76

exhilarating. An earlier study shown that T_g increased as a function of crystallinity in the case of branched PE.[39] One can thus conclude that particle size is taking a dominating factor with change in crystallinity of PP nanoparticles to affect the T_g. Hence, PP particles with size ranging from several nanometers to several micrometers are spherical in nature with different T_g values. In the last two decades, few theoretical models have been developed to understand the finite size effect on T_g. The T_g of a free-standing polymer decreases as its thickness of thin film decreases. The T_g of a substrate-supported film can decrease or increase depending on the strength of chemical bonding and chemical interaction between support film and the thickness of the film.[40–44] The increase in T_g of polymer particles or thin film can expect when the chemical interaction between substrate and the film is stronger then Van der Waals force or hydrogen bonding between the polymer chains and the substrate. Ding et al.[45] prepared PS micro particles by freeze drying and showed that the microparticles have the lower T_g than that of bulk PS. But, polymers are of arbitrary coil configuration. When PP chain exists as a single molecular form, the root mean square Z-average ($\langle s^2 \rangle_z^{1/2}$) would be about 53 to 118 nm (by light scattering measurement) depending on the MW.[46] If the single chain is packed with density similar to that of bulk, the diameter of the spheroids would be less than 100 nm. Further, our previous investigation showed that with a decrease in the particle size there is a noticeable trend of increase in crystallinity (Figs. 5 and 6). This investigation shows that the PP nanoparticle is more crystalline with higher T_g.

Now the question is how T_g is related with the finite size effect of PP particle. To find out the

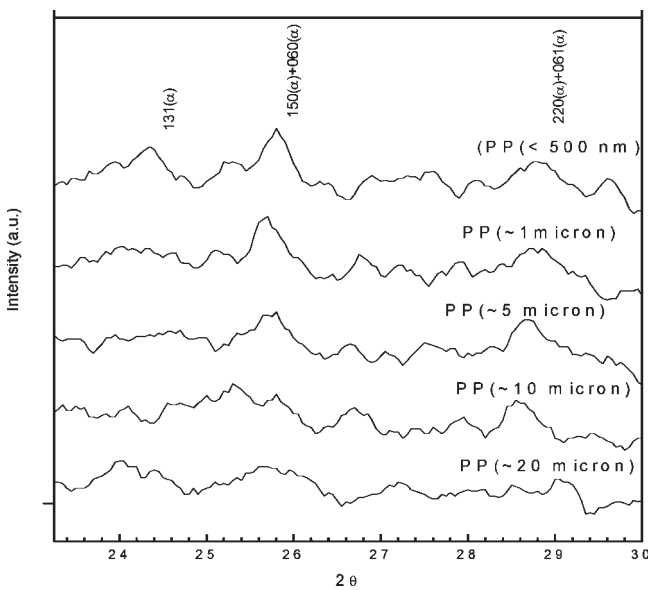

Figure 6 X-ray powder diffraction patterns for PP micro- and nanoparticles, (2θ = 23.5°–30°).

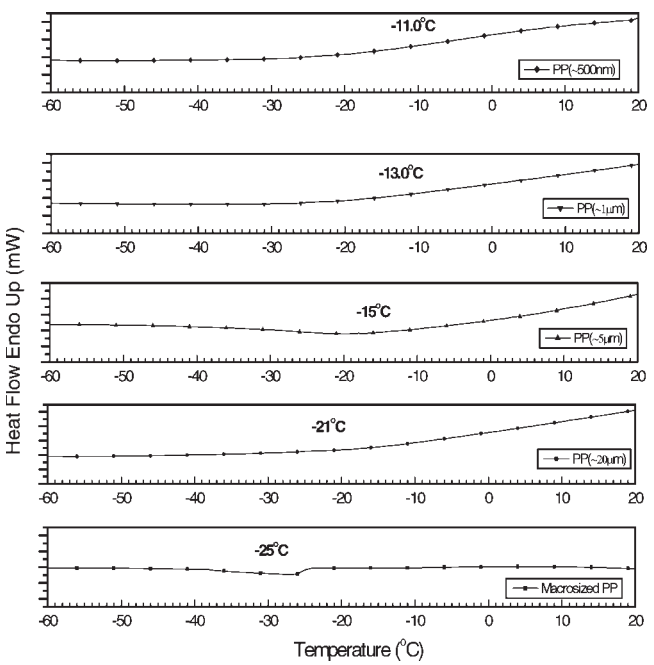

Figure 7 DSC graph of PP particles. The scanning rate was 10°C/min from −100 to 40°C.

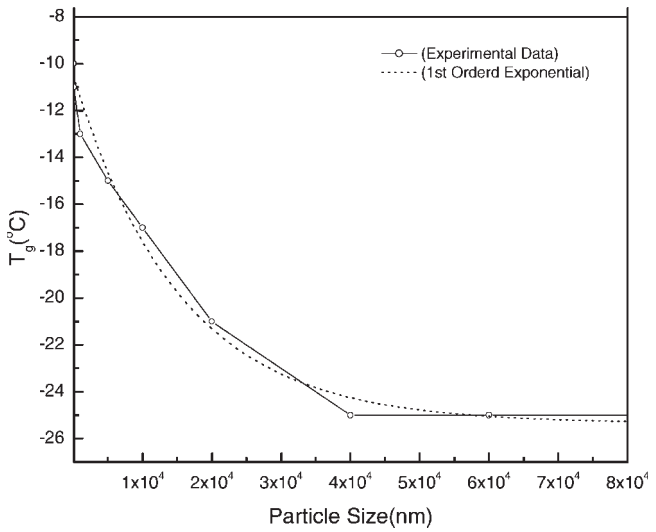

Figure 8 Effect of particle size on T_g for PP particles.

answer, T_g data is plotted as a function of particle size in Figure 8. The continuous line represents the experimental data and the dotted line is the 1st order exponential nature (best fit). This shows that T_g increases as the particle size decreased and explained by eq. (3).[47]

$$\ln\frac{T_{gp}}{T_{gb}} = \frac{kN}{\Delta C_p}(N^{(x/3)} + N^{-2}\ln 2) \tag{3}$$

where subscripts g, p, and b stand for glassy state, particle, and bulk respectively. N, k, and x are degree of polymerization, Boltzmann const., and a const. 5/3, respectively. This shows the particles will have higher T_g than that of bulk. Thus, the theoretical justification agrees well with our investigational data. As the particle size decreases to micron and nanoscale, the configuration entropy of PP particles decreases and becomes a lower value, with further reducing the particle size towards its single chain; T_g will be elevated. However, physical interpretation of the lowering of configuration entropy because of the miniaturization of particle size addresses to (1) highest possibility of chain entanglement and interlocking, (2) limited number of chain ends to the surface, (3) restricted chain mobility, and (4) enhanced crystallinity of PP spherical nanoparticles are the causes of enhancement of T_g.

To evaluate the micromechanical properties, 10–15 force–distance curves were measured with various indentation depths for PP particles in the nanometer range using AFM. All force–distance curves (Fig. 9) obtained show a sharp contact point, repulsive range in the approaching part, pull-off point in the retracting cycle. The elastic modulus of PP particles are fairly measured over the entire range of indentation depths and gives the consistent results in between 0.20–0.18 GPa (within ± 20% error) using eq. (4).[48]

$$\frac{dF}{dh} = \frac{2A^{1/2}}{\pi^{1/2}} \times E^* \tag{4}$$

where, $\frac{1}{E^*} = \frac{1-\nu_1^2}{E_1} + \frac{1-\nu_2^2}{E_2}$, the composite elastic modulus; E_1, E_2 (140 GPa), ν_1 (0.33), ν_2 (0.27), Young's moduli and Poisson's ratio of a sample and an tip respectively; F, normal load; A, contact area (tip diameter, r = 10 nm) and h, the indentation depth. Figure 10(a,b) shows 2D and 3D views of nanosized PP, whose particle size is ~ 75 nm. The surface profile diagram of this nanosized PP is also shown in Figure 10(c). The surface roughness (RMS, root mean square) was calculated from this diagram and is ~ 10 Å. To understand the effect of particle size on surface roughness of PP, measurements were extended over a wide range of particles. The results are plotted in Figure 10(d). It shows that it increases with an increase of particle size upto 400 nm, and after that it remains constant.

CONCLUSIONS

The following conclusions have been drawn from the present investigation:

1. Particle size distribution demonstrates the particle size of nanopolymer, PP is within a range of

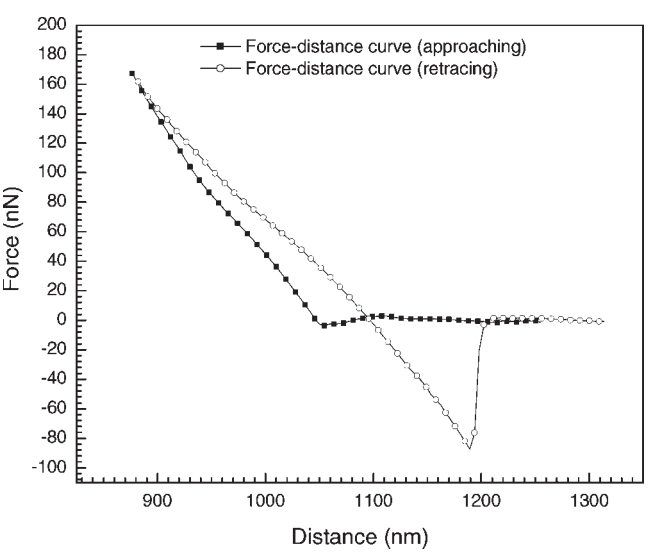

Figure 9 Force–distance data for the PP particles in an approaching-retracting cycle measured in AFM using mica as a substrate and silicon tip of V shape with force constant 0.5 N/m. Retraction of the tip lead to hysteresis caused by adhesion force (negative).

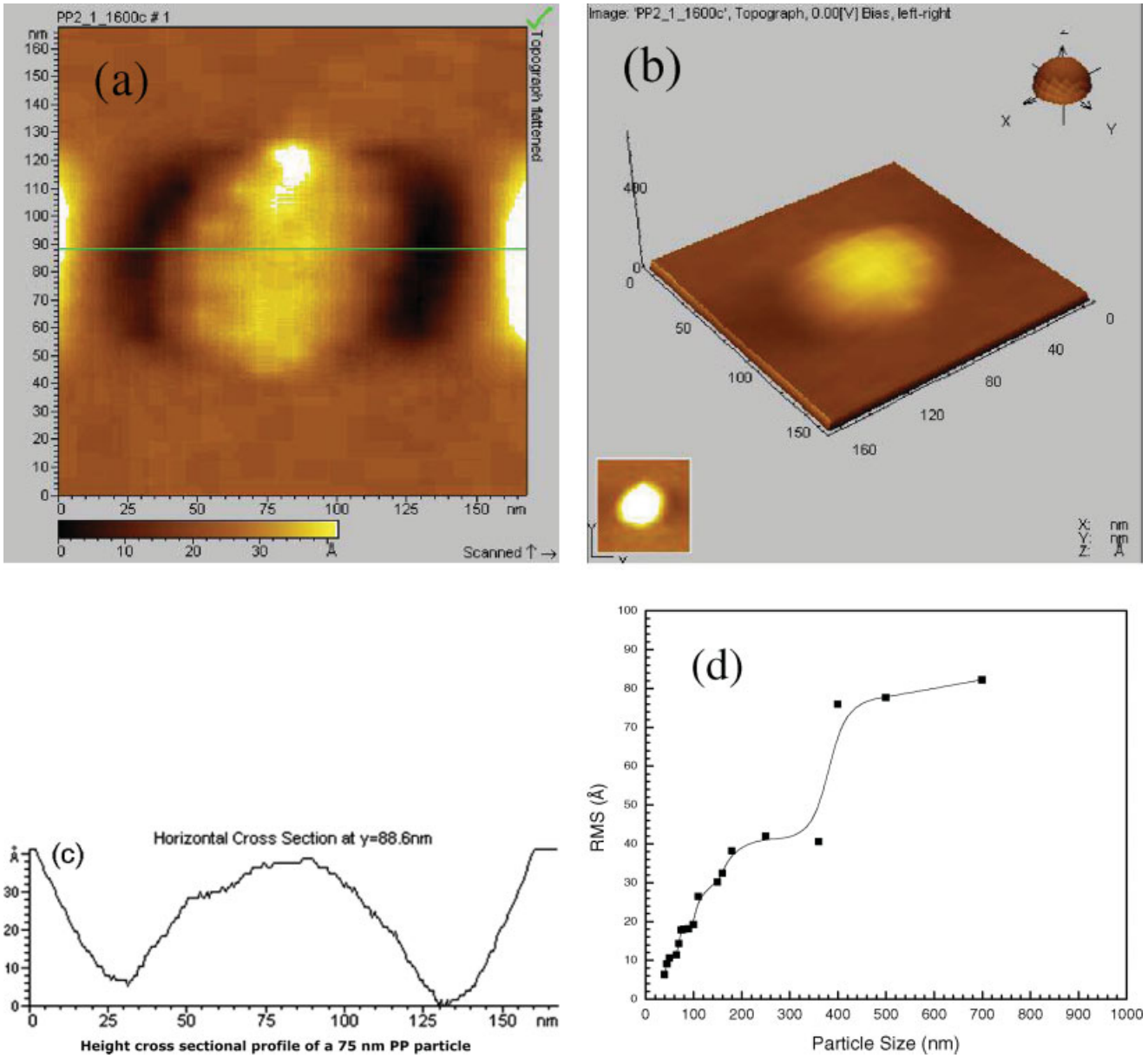

Figure 10 (a) AFM topograph of a 75 nm PP particle. (b) 3D view of AFM for a 75 nm PP particle. (c) Height cross-sectional profile of a 75 nm PP particle. (d) Effect of particle size on surface roughness. [Color figure can be viewed in the online issue, which is available at www.interscience.wiley.com.]

40–60 nm in diameter supported through AFM, 44–55 nm observed through TEM and 60–200 nm noticed through SEM.
2. AFM, TEM, and SEM results show that the nanopolymer is spherical in nature.
3. Infrared spectroscopy studies of macro PP and nano PP indicate that both polymers have same chemical structure and chemical bonding.
4. XRD studies reveal that the nanopolymer is more crystalline in nature.
5. T_g increases with a decrease of particle size, whereas surface roughness increases with an increase of particle size.
6. AFM studies show that the Young's modulus of nanosized particle varies from 0.2 to 0.18 GPa.

References

1. Harel, E.; Meltzer, S. E.; Requicha, A. A. G.; Thompson, M. E.; Koel, B. E. Nano Lett 2005, 12, 2624.
2. Lu, C.; Wang, Q. J Mater Process Technol 2004, 145, 336.
3. Metin, D.; Tihminlioğlu, F.; Balköse, D.; Ülkü, S. Compos Part A: Appl Sci Manuf 2004, 35, 23.
4. Hadal, R.; Dasari, A.; Rohrmann, J.; Misra, R. D. K. Mater Sci Eng A 2004, 380, 326.
5. Salis, A.; Sanjust, E.; Solinas, V.; Monduzzi, M. J Mol Catal Part B: Enzymatic 2003, 24/25, 75.

6. Adamczak, M.; Bednarski, B. Process Biochem 2004, 39, 1347.
7. Yoshida, M.; Shimosaka, A.; Shirakawa, Y.; Hidaka, J.; Matsuyama, T.; Yamamoto, M. Powder Technol 2003, 135/136, 23.
8. Hamskog, M.; Ahlblad, G.; Färnert, G.; Gijsman, P.; Terselius, B.; Polym Test 2003, 22, 363.
9. Al-Duri, B.; Goddard, R.; Bosley, J. J Mol Catal Part B: Enzymatic 2001, 11, 825.
10. Sokól, W. Biochem Eng J 2001, 8, 203.
11. Jerrim, K. L.; Hughes, J. F.; McKechnie, M. T. J Electrostat 2001, 53, 39.
12. Kacprzyk, R.; Gajewski, J. B. J Electrostat 2001, 51/52, 124.
13. Wilken, R.; Holländer, A.; Behnisch, J. Surf Coat Technol 1999, 116–119, , 991.
14. Bidan, G. Sens Actuat B 1992, 6, 45.
15. Norris, I. D.; Shaker, M. M.; Ko, F. K.; MacDiarmid, A. G. Synth Met 2000, 114, 2.
16. Peyser, L. A.; Vinson, A. E.; Bartko, A. P.; Dickson, R. M. Science 2001, 291, 103.
17. Kim, P.; Lieber, H. M. Science 1999, 286, 2148.
18. Sitti, M.; Hashimoto, H. IEEE/ASME Trans Mechatronics 2000, 5, 199.
19. Yi, D. K.; Seo, E.; Kim, D. Langmuir 2002, 18, 5321.
20. Joannopoulos, J. D.; Villeneuve, P. R.; Fan, S. Nature 1997, 386, 143.
21. Lu, Y.; Yin, Y.; Xia, Y. Adv Mater 2001, 13, 415.
22. Kietze, T.; Neher, D.; Landfester, K.; Montenegro, R.; Guentner, R.; Scherf, U. Nat Mater 2003, 2, 408.
23. Hamley, I. W. Angew Chem Int Ed 2003, 42, 1692.
24. Cölfen, H.; Mann, S. A. Angew Chem Int Ed 2003, 42, 2350.
25. Qi, K.; Ma, Q.; Remsen, E. E.; Clark, C. G., Jr.; Wooley, K. L. J Am Chem Soc 2004, 126, 6599.
26. Zhang, G.; Niu, A.; Peng, S.; Jiang, M.; Tu, Y.; Li, M.; Wu, C. Acc Chem Res 2001, 34, 249.
27. Zhang, Q.; Remsen, E. E.; Wooley, K. L. J Am Chem Soc 2000, 122, 3642.
28. Buetuen, V.; Billingham, N. C.; Armes, S. P. J Am Chem Soc 1998, 120, 12135.
29. Zhou, J.; Li, Z.; Liu, G. Macromolecules 2002, 35, 3690.
30. Harth, E.; Van Horn, B.; Lee, V. Y.; Germack, D. S.; Gonzales, C. P.; Miller, R. D.; Hawker, C. J Am Chem Soc 2002, 124, 8653.
31. Kar, K. K.; Paik, P. Indian Pat. 2503/DEL/2004 (2004).
32. Kar, K. K.; Paik, P. Indian Pat. 3161/DEL/2005 (2005).
33. Xu, X. J.; Chew, C. H.; Siow, K. S.; Wong, M. K.; Gan L. M. Langmuir 1999, 15, 8067.
34. Zhu, X.; Yan, D.; Fang, Y. J Phys Chem B 2001, 105, 12461.
35. Zhu, X.; Fang, Y.; Yan, D. Polymer 2001, 42, 8595.
36. De Rosa, C.; Auriemma, F.; Circelli, T.; Waymouth, R. M. Macromolecules 2002, 35, 3622.
37. Machado, G.; Denardin, E. L. G.; Kinast, E. J.; Goncalves, M. C.; de Luca, M. A.; Teixeira, S. R.; Samios, D. Eur Polym J 2005, 41, 129.
38. Hermans, P. H.; Weidingeer, A. Makromol Chem 1961, 44–46, 24.
39. Bartenev, G. M.; Remizova, A. A.; Kuleshov, I. V.; Martynov, M. A. Vysokomol Soedin A 1973, 15, 2480.
40. Forrest, J. A.; Dalnoki-Veress, K.; Stevens, J. R.; Ducher J. R. Phys Rev Lett 1996, 77, 2002.
41. Jérōme, B.; Commandeur, J. Nature 1997, 386, 589.
42. DeMaggio, G. B.; Frieze, W. E. Phys Rev Lett 1997, 78, 1524.
43. Kajiyama, T.; Tanaka, K.; Takahara, A. Macromolecules 1999, 28, 3482.
44. Frank, C. W.; Rao, V.; Despotopoulou, M. M.; Pease, R. F. W.; Hinsberg, W. D.; Miller, R. D.; Rabolt, J. F. Science 1996, 273, 912.
45. Ding, J.; Xue, G.; Dia, Q.; Cheng, R. Polymer 1993, 34, 3325.
46. Brandrup, J.; Immergut, E. H. Polymer Hand Book, 3rd ed.; Wiley: New York, 1989; Vol. 23.
47. Mi, Y.; Xue, G.; Wang, X. Polymer 2002, 43, 6701.
48. Johnson, K. L. Contact Mechanics; Cambridge University Press: Cambridge, 2001; p 92.